Japanese Journal of Applied Physics **60**, 110501 (2021)
https://doi.org/10.35848/1347-4065/ac2918

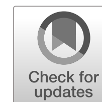

Nanoscale and quantum engineering of III-nitride heterostructures for high efficiency UV-C and far UV-C optoelectronics

Xianhe Liu[1,2*], Ayush Pandey[1], and Zetian Mi[1]

[1]*Department of Electrical Engineering and Computer Science, University of Michigan, Ann Arbor, 1301 Beal Ave., Ann Arbor MI 48109, United States of America*
[2]*Guangzhou Institute of Technology, Xidian University, Guangzhou 511555, People's Republic of China*

*E-mail: liuxianhe@xidian.edu.cn

Received August 7, 2021; revised September 18, 2021; accepted September 21, 2021; published online October 12, 2021

We present an overview of some recent advances of nanoscale and quantum engineering of III-nitride heterostructures that are relevant for the development of high efficiency ultraviolet (UV)-C and far UV-C optoelectronic devices, including light emitting diodes and laser diodes. We show that relatively efficient p-type conduction of AlN and Al-rich AlGaN can be achieved in nearly dislocation-free nanostructures, or through in situ Fermi-level control during the growth of epilayers. High luminescence emission efficiency in the deep UV can be realized by exploiting strong quantum confinement of charge carriers, through either the formation of quantum dot-like nanoclusters or monolayer quantum wells. Moreover, the three-dimensional quantum confinement of charge carriers can drastically reduce the transparency carrier density of ultrawide bandgap semiconductors, leading to electrically pumped mid and deep UV laser diodes with ultralow threshold operation.
© 2021 The Japan Society of Applied Physics

1. Introduction

Ultraviolet (UV)-C light, in the wavelength range of ~200–280 nm, has emerged as a highly attractive method for disinfection, compared to conventional chemical treatment, for its capability of damaging the DNA and RNA of viruses.[1,2] Traditional UV-C light sources are dominantly mercury lamps and excimer lamps. The operation of these lamps involves the use of toxic chemicals that are harmful for the environment and human health. These lamps are also bulky and inefficient. Therefore, all solid-state AlGaN based UV-C emitters have received significant attention. To date, AlGaN UV LEDs exhibit very low efficiency, particularly for emission wavelengths below 280 nm,[3–11] which has been largely limited by the low crystalline quality due to the large lattice mismatch, poor p-type conduction, and inefficient light extraction related to the in-plane transverse-magnetic polarized emission of Al-rich AlGaN alloys. These critical issues, together with the intrinsically large transparency carrier density of ultrawide bandgap semiconductors, have also prevented the realization of low threshold mid and deep UV laser diodes.[12–15] The recently reported AlGaN quantum well laser diodes operating below 300 nm have threshold current density in the range ~15–70 kA cm^{-2} under extremely short pulsed operation.[14]

Recent studies suggest that some of these critical issues can be addressed through nanoscale and quantum engineering of III-nitride heterostructures.[15–21] Due to the efficient strain relaxation, dislocation-free III-nitride nanostructures can be epitaxially grown directly on foreign substrates.[22,23] Recent advances in selective area epitaxy have further shown that their properties can be precisely controlled, resulting in superior quality nanocrystals that are extremely device worthy.[24–26] Also due to efficient strain relaxation, Al (or Ga)-substitutional Mg formation energy is significantly reduced in defect-free nanocrystals, compared to conventional film structures.[20] Free hole concentration up to 6×10^{17} cm^{-3} was measured in Mg-doped AlN nanocrystals.[27] Significantly improved p-type conduction has also been achieved in Al-rich AlGaN through the use of a new epitaxy process, that is in situ tuning of the surface Fermi level during epitaxy, which can enhance the incorporation of Mg-acceptors without the formation of extensive compensating defects.[18] These advances have enabled the realization of tunnel junction (TJ) UV-C and far UV-C LEDs with unprecedented performance, including high external quantum efficiency (EQE) (>10%) and high electrical efficiency.[19,20] Recent studies further suggest that high luminescence emission efficiency in the deep UV can be realized by exploiting strong quantum confinement of charge carriers, through either the formation of quantum dot-like nanoclusters or monolayer quantum wells.[28,29] Significantly, the three-dimensional quantum confinement of charge carriers can drastically reduce the transparency carrier density of ultrawide bandgap semiconductors, which, together with the relatively efficient p-type conduction, can lead to electrically pumped mid and deep UV laser diodes with ultralow threshold operation.[18,30,31]

In this article, we present an overview of some recent advances of nanoscale and quantum engineering of III-nitride heterostructures that are relevant for the development of UV-C and far UV-C LEDs and laser diodes. Efficient incorporation of p-type Mg dopant and relatively low p-type resistivity were achieved for Al-rich AlGaN as well as AlN by using nanostructure and/or by pinning the surface Fermi level with metal–semiconductor junction during epitaxy. Three-dimensional quantum confinement was realized in both nanostructures and planar epilayers. Such structural improvements, together with optimized device design including TJ, electron blocking layers, and photonic crystals, have led to the realization of relatively efficient UV-C and far UV-C LEDs and low threshold laser diodes.

2. Experimental methods

AlGaN heterostructures, in both nanocrystal and conventional epilayer forms, were grown using plasma-assisted molecular beam epitaxy (MBE) in this study. Early studies on III-nitride nanocrystals by MBE often relied on the spontaneous formation under nitrogen-rich epitaxy conditions.[22,32–34] Recent advances of selective area epitaxy have enabled the development of site-controlled AlGaN nanocrystals, shown in Fig. 1.[25,35] In this process, the growth mask consisting of a metal or dielectric

© 2021 The Japan Society of Applied Physics

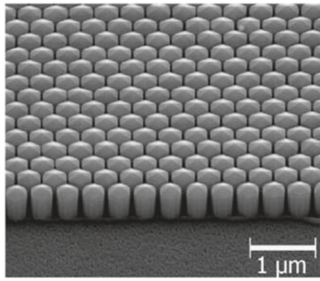

Fig. 1. A scanning electron microscopy image of GaN/AlGaN nanocrystals formed by selective area epitaxy. (Reproduced with permission from Ref. 24.)

layer is firstly deposited on the substrate and then patterned by electron beam lithography and dry etching. Under optimized growth conditions, epitaxy only occurs in the regions where the growth mask is etched and the substrate is exposed. The polarity of the homo, or hetero-epitaxially grown nanocrystals is determined by the polarity of the template. Both metal-polar and N-polar nanocrystals have been demonstrated.[25,36–40] In the presented study, selective area epitaxy of GaN is performed on GaN templates using a thin layer of Ti as the mask. Nanoscale engineering of III-nitride heterostructures can also be achieved by using a slightly metal-rich epitaxy condition. These conditions result in the formation of Ga-rich nanoclusters,[41–43] which can increase the internal quantum efficiency due to the three-dimensional quantum confinement. Using metal–semiconductor junction-assisted epitaxy, a thin liquid Ga layer forms a metal–semiconductor junction at the growth front, schematically shown in Fig. 2(a), which leads to the pinning of the Fermi level away from the valence band at the growth front, shown in Fig. 2(b). Figure 2(c) shows the formation energy for the Mg acceptor using metal–semiconductor junction assisted epitaxy, as well as conventional epitaxy in nitrogen-rich

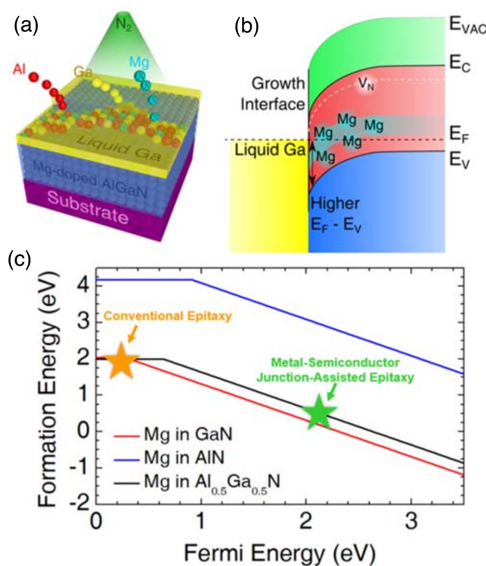

Fig. 2. (Color online) (a) Schematic of the surface migration dynamics during metal–semiconductor junction assisted epitaxy. (b) Energy band diagram at the growth front during the metal–semiconductor junction assisted epitaxy. (c) Variation of the formation energy of Mg substitution in GaN, AlN, and $Ga_{0.5}Al_{0.5}N$ with the separation between the Fermi level and the valence band. (All reproduced with permission from Ref. 18. Copyright 2019 by the American Physical Society.)

conditions. The increased separation between the Fermi level and the valence band edge reduces the formation energy for Mg acceptors, promoting their incorporation into the crystal lattice, while simultaneously increasing the formation energy of compensating defects.[44–46] Therefore, these growth conditions can dramatically improve the p-type dopant incorporation in AlGaN.[18,47,48]

LEDs and laser diodes were fabricated using standard photo/e-beam lithography, etching, and contact metallization techniques. Structural characterization was performed using high-resolution scanning transmission electron microscopy (STEM), including high-angle annular dark-field (ADF) imaging and electron energy-loss spectroscopy (EELS) spectrum imaging. Optical properties were measured using a 193 nm excimer laser as the excitation source. Photoluminescence (PL) and electroluminescence (EL) spectra were collected by a set of standard lenses, a microscope objective lens, or a fiber and directed into a monochromator equipped with a charge-coupled device. A Keithley 2400 source meter was used to measure current–voltage (*IV*) characteristics. The device output power was measured using a Newport power meter and a Newport silicon detector.

3. Results and discussion

3.1. Results

3.1.1. p-type conduction of AlN and Al-rich AlGaN. Despite the large activation energy for Mg dopants, relatively efficient p-type conduction has been demonstrated by exploiting the reduced Ga (Al) substitutional Mg-dopant formation energy for nanocrystals. First principle calculation revealed that the incorporation of Mg in AlN on the *m*-plane sidewalls of nanocrystals was more efficient than in the bulk, due to the efficient strain relaxation.[20] In addition, the N-rich condition used for the growth of nanocrystals can significantly promote the incorporation of Mg. With the presence of high concentration of Mg, discrete Mg levels start to interact forming an impurity band. PL measurements of Mg doped AlN nanocrystals reveal a pronounced peak at 235 nm, which is well separated from the peak at ~207 nm from the excitonic transition of undoped AlN nanocrystals, shown in Fig. 3(a).[49] The energy separation of 0.5–0.6 eV between them agrees well with the activation energy for Mg-acceptors in AlN.[27,50] Such a pronounced peak was hardly measured from conventional Mg doped AlN epilayers at room temperature, confirming the enhanced Mg incorporation and superior quality of AlN nanostructures. Since the Mg acceptor related transition peak exhibited a large broadening, the energy separation between the top of the valence band and the lowest Mg energy states was significantly smaller than the activation energy (~500–600 meV), suggesting a significant reduction of activation energy for a portion of Mg dopants and consequently improved p-type conduction.

Electrical measurement of the hole concentration in Mg-doped AlN nanocrystals was also performed. The temperature-dependent hole concentrations for two Mg-doped AlN nanocrystal samples are shown in Fig. 3(b).[52] For the sample with a lower Mg concentration, the hole concentration increased monotonically with temperature, while the sample with higher Mg concentration exhibited a more complicated behavior. The hole concertation decreased with temperature in the regime below 550 K and then increased with temperature in the higher

 © 2021 The Japan Society of Applied Physics

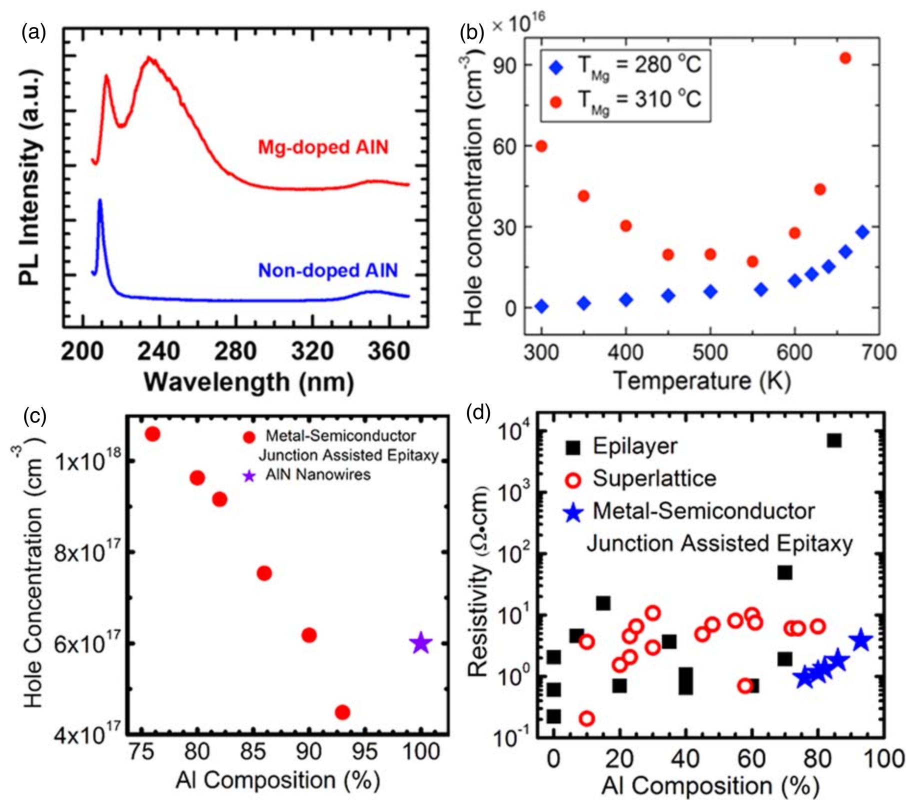

Fig. 3. (Color online) (a) PL spectra of a non-doped AlN nanocrystal sample and a Mg-doped AlN nanocrystal sample at room temperature. (b) Temperature dependent hole concentration in heavily Mg-doped (red circles) and moderately Mg-doped (blue diamonds) AlN nanocrystals. (c) Hole concentrations achieved with metal–semiconductor junction assisted epitaxy and nanowire structure for various Al compositions. (d) Resistivities of Mg-doped AlGaN epilayers achieved by us and other groups. [(a) Reproduced with permission from Ref. 49 (b) reproduced from Ref. 51 with a Creative Commons Attribution (CC BY) license. (c) and (d) Reproduced with permission from Ref. 18. Copyright 2019 by the American Physical Society.]

temperature regime. The reduction of hole concentration with temperature below 550 K is explained by the two-band conduction model, in which the overall measured number of holes decreases at elevated temperatures due to ionization from the impurity band into the valence band. The hole conduction in the valence band started to dominate as the temperature was sufficiently high (>550 K), which led to the increase of measured hole concentration with temperature. High Mg concentration was further confirmed by a very small activation energy of 23 meV which was characteristic of hopping conduction in the impurity band formed by high dopant concentration.[16)]

Studies by us, as well as others, have shown that tuning the Fermi level during epitaxial growth can produce more efficiently doped material and reduce point defect incorporation.[18,53–55)] For the case of $Al_{0.5}Ga_{0.5}N$, the presence of a thin liquid gallium layer on the growth front results in an increase in the separation between the Fermi level and the valence band from ~0.12 to ~2.2 eV. This leads to a decrease in the formation energy of the Mg acceptor from ~2 to ~0.43 eV. Furthermore, first principle calculations have indicated that typical compensating defects, such as nitrogen vacancies, can play a significant role in limiting free hole concentration,[46,56,57)] which has a reduced formation energy with decreasing separation between the Fermi level and valence band, such as in Mg-doped AlGaN. It was found that, by increasing the separation between the Fermi level and valence band through metal–semiconductor junction assisted epitaxy, dopant compensation can be effectively minimized. Therefore, high concentrations of Mg dopants can be incorporated in high Al content AlGaN, which leads to the presence of a Mg impurity band enabling efficient hole transport at room temperature. Figure 3(c) plots the hole concentrations measured at room temperature for high Al content AlGaN epilayers, with concentrations of over 10^{17} cm^{-3} for Al contents of up to 90%. Al-rich AlGaN epilayers, with resistivity values below 1 Ω·cm for $Al_{0.75}Ga_{0.25}N$ and ~4 Ω·cm for $Al_{0.9}Ga_{0.1}N$ have been measured, shown in Fig. 3(d). These values are several orders of magnitude lower than those previously reported values for AlGaN epilayers with such Al contents. Deep UV LEDs grown using this method showed a significant improvement in EQE, and lower turn-on voltage, as compared to devices grown using conventional epitaxy.[18)]

3.1.2. Three-dimensional quantum confinement of charge carriers of Al-rich AlGaN. Carrier localization plays a key role in high efficiency emission of high performance InGaN blue LEDs despite high densities of threading dislocations.[58,59)] Recently, three-dimensional quantum confinement has been demonstrated in both AlGaN nanocrystals and planar epilayers with high Al contents. Shown in Fig. 4(a) are a high magnification high angle ADF image (left panel) and a distribution map of Ga (right panel) that was concurrently collected from the same region of an AlGaN nanowire.[15)] The relatively bright regions in the ADF image coincide with the relatively strong signals in the Ga elemental map, confirming the presence of local compositional fluctuations and Ga-rich clusters. The local fluctuation of Ga content is estimated to be 5%–10%. The Ga-rich clusters exhibited thicknesses between a single atomic layer and ~2 nm along the *c*-axis and lateral

 © 2021 The Japan Society of Applied Physics

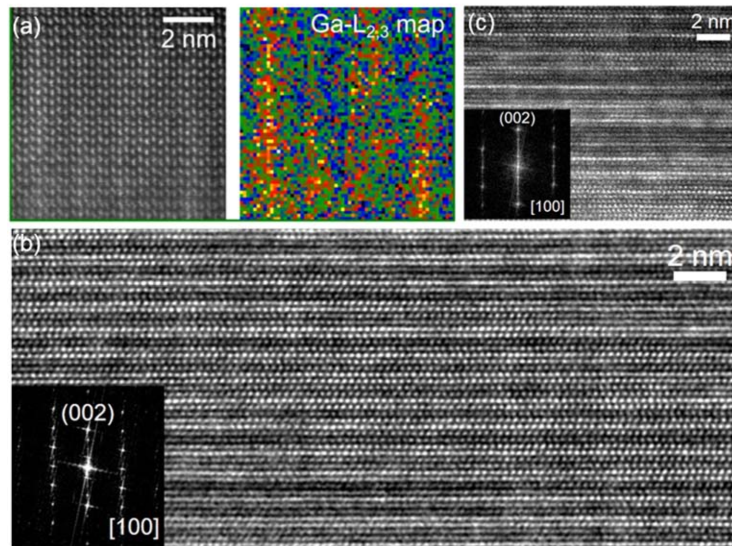

Fig. 4. (Color online) (a) The ADF signal from EELS spectrum imaging (left) and the Ga-map (right) displayed in temperature-scale exhibiting a direct correspondence with the ADF signal. (b) and (c) Atomic scale HAADF-STEM images of an $Al_{0.75}Ga_{0.25}N$ layer showing the presence of nanoscale Ga-rich layers due to compositional variation. The brighter regions correspond to the higher Ga content. [(a) Reproduced with permission from Ref. 15. Copyright 2015 American Chemical Society. (b) and (c) reproduced from Ref. 41, with the permission of AIP Publishing.]

dimension in the range of ~2–10 nm. Such atomic scale Ga-rich regions exhibited quantum-dot like features providing three-dimensional quantum confinement of carriers. The formation of such atomic structures is attributed to both spontaneous chemical ordering and anisotropic surface migration from sidewalls.[15)]

During MBE growth of AlGaN epilayers, the use of a slightly metal-rich condition can result in the presence of significant compositional ordering and the formation of Ga nanoclusters in the material as shown in Figs. 4(b) and 4(c). These clusters provide sites where carriers can be localized, and the three-dimensional confinement of carriers enables highly efficient radiative recombination.[15,43)] The band structure fluctuations induced by the Ga nanoclusters can lead to enhanced modal gain at wavelengths below 250 nm, enabling extremely low transparency thresholds which is critical for low threshold UV laser diodes.[30,31)] The EL of such devices has been shown to be dominated by emission from these clusters, which resulted in highly stable emission peak with negligible change over orders of magnitude of injection currents.[19,41)]

Extreme quantum confinement was further studied using monolayer GaN in AlN matrix. Distinct emission peaks at ~238 nm and 270 nm were measured from single and double monolayer GaN in AlN, respectively, which was in good agreement with previous theoretical calculations.[60)] The integrated PL intensity from monolayer GaN was found to linearly increase with the excitation intensity, indicating strong suppression of Auger recombination and the nature of excitonic emission at room temperature.[61–63)] The exciton binding energy was estimated to be ~200 meV, which was derived from the difference between the measured optical bandgaps and the calculated electronic bandgaps of a series of GaN/AlN heterostructures with different GaN and AlN barrier thicknesses. This exciton binding energy is nearly ten times higher than that in bulk GaN and enables stable excitonic emission at room temperature.

3.1.3. UV-C and far UV-C LEDs. The significantly reduced dislocations and relatively efficient p-type conduction of AlN-based nanocrystals offer a unique opportunity for improving the performance of far UV-C LEDs. A relatively high IQE (~80%) was measured in AlN nanocrystals.[20)] AlN nanocrystal LEDs operating at ~210 nm exhibited a turn-on voltage as low as 6 V, which was significantly smaller than that of previously reported planar AlN epilayer devices.[64)] Even under cryogenic temperatures, there was only a slight increase in the turn-on voltage, showing that the conduction was not sensitive to temperature due to the hole hopping conduction.[65)] More recently, hexagonal boron nitride (h-BN) was introduced to improve the performance of AlN nanocrystal LEDs because of its better p-type conductivity than Mg-doped AlN.[66)] The p-type conductivity is attributed to the formation of point defects, e.g. boron vacancies, that are shallow acceptors.[67–69)] The device structure is similar to AlN nanocrystal LEDs except that the Mg-doped AlN segment is replaced by h-BN grown under N-rich condition to promote the formation of acceptor-like boron vacancies as shown in the inset of Fig. 5(a).[17)] The *IV* characteristics exhibited a turn-on voltage of only 5.5 V as shown in Fig. 5(a) and the leakage current under reverse bias was negligible. The EL emission spectra were measured for current densities from 5 to 70 A cm^{-2}, shown in Fig. 5(b). A pronounced peak from excitonic transition at ~210 nm was observed together with a minor peak at around 214 nm from longitudinal optical phonon replica, which suggests the superior crystalline quality.[70)] A comparison in terms of output power between the h-BN/AlN LED and the AlN nanocrystal LED is shown in Fig. 5(c). The h-BN/AlN LED output power was more than 10 times higher than that of the AlN homojunction device. This drastically enhanced output is the direct consequence of better hole transport and injection and stronger carrier confinement.[17)] By incorporating Ga under different growth temperatures, the composition can be readily tuned to yield EL peak wavelengths between 236 and 280 nm without emission from any defects as shown in Fig. 5(d).[71)]

Hole injection into the active region is also one of the bottlenecks for achieving high performance AlGaN UV-C

 © 2021 The Japan Society of Applied Physics

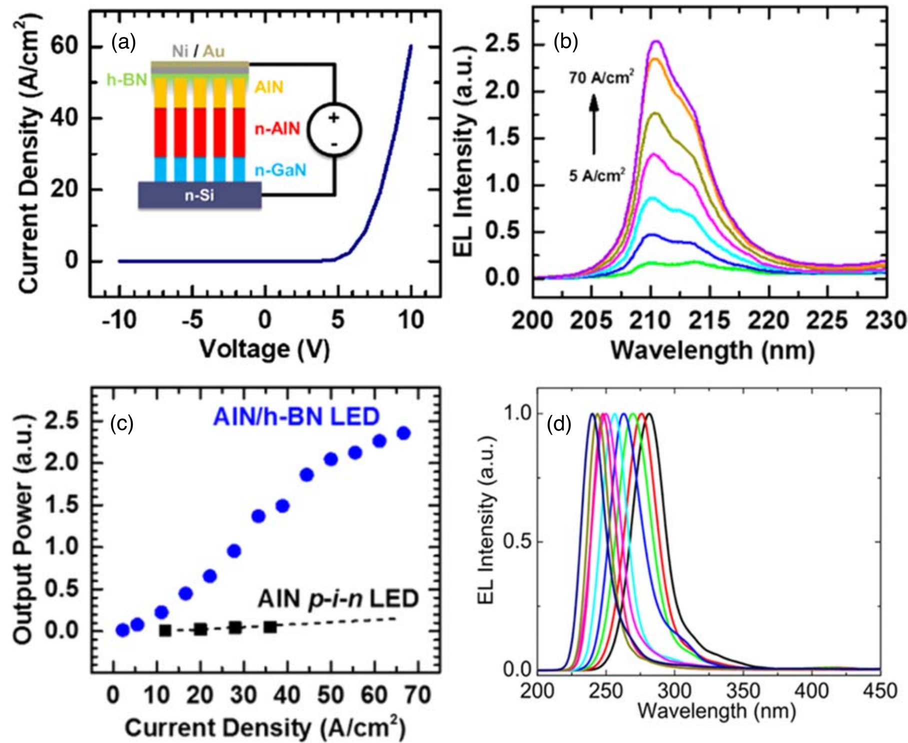

Fig. 5. (Color online) (a) *IV* characteristics of a h-BN/AlN LED at room temperature. Inset: Schematic of the LED structure. (b) EL spectra of the h-BN/AlN LED measured under injection current densities between 5 and 70 A cm^{-2}. (c) Output power versus injection current for the h-BN/AlN LED. The black dashed line indicates the linearly extrapolated output power of an equivalent AlN p-i-n homojunction LED at higher current densities. (d) Tuning of emission wavelength of AlGaN nanocrystal LEDs. [(a)–(c) Reproduced with permission from Ref. 17. Copyright 2017 American Chemical Society. (d) Reproduced from Ref. 71 with a Creative Commons Attribution (CC BY) license.]

LEDs. It is demonstrated that tunnel injection of nonequilibrium holes can lead to an enhanced hole injection efficiency.[72–76] We designed and developed a metal/semiconductor TJ consisting of a n^{++}-GaN/Al/p^{++}-AlGaN structure in AlGaN nanocrystal LEDs as shown in the inset of Fig. 6(a).[77] The *IV* characteristics were compared with those of a standard p-i-n LED in Fig. 6(a). While the turn-on voltage was similar for these two structures, the differential resistance above the turn-on voltage was estimated to be ~35 Ω for the TJ LED, significantly lower than that of the p-i-n LED. The EL spectra exhibit a single pronounced peak at 275 nm, shown in Fig. 6(b). The TJ LED also exhibits nearly two orders of magnitude higher output power than the standard p-i-n device, shown in Fig. 6(c). By increasing the Al content of the structure, AlGaN nanocrystal TJ LEDs emitting at 240 nm also exhibited significantly improved performance.[78]

More recently, with the use of TJ, AlGaN quantum well LEDs with EQE up to 11% and 7% have been demonstrated at 265 nm and 255 nm, respectively.[19,41] These devices utilized polarization-engineering to achieve efficient tunneling. A thin GaN layer sandwiched between the highly doped p-type and n-type AlGaN layers results in a massive increase in interband tunneling of carriers due to the large electric fields generated by the strong spontaneous and piezoelectric polarization. This enabled highly efficient device operation, with the EQE of a device having 255 nm emission shown in Fig. 7(a). The devices had extremely

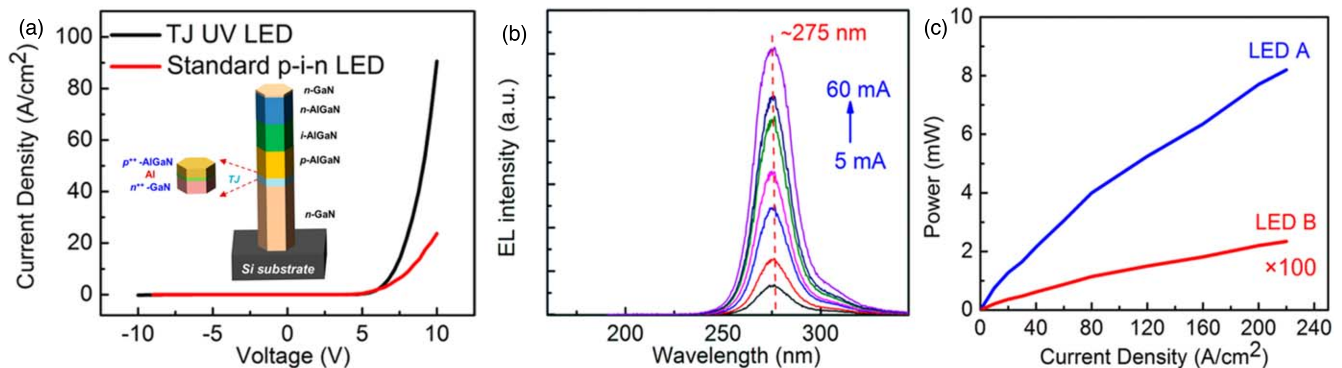

Fig. 6. (Color online) (a) *IV* characteristics of an Al TJ AlGaN nanocrystal LED and a standard p-i-n AlGaN nanocrystal LED. Inset: Schematic of the Al TJ AlGaN nanocrystal LED structure. (b) EL spectra of the Al TJ AlGaN UV LED under varying injection currents. (c) Output power versus injection current density for the Al TJ nanocrystal LED (LED A) and a standard p-i-n nanocrystal LED (LED B). (All reproduced with permission from Ref. 77 Copyright 2017 American Chemical Society.)

© 2021 The Japan Society of Applied Physics

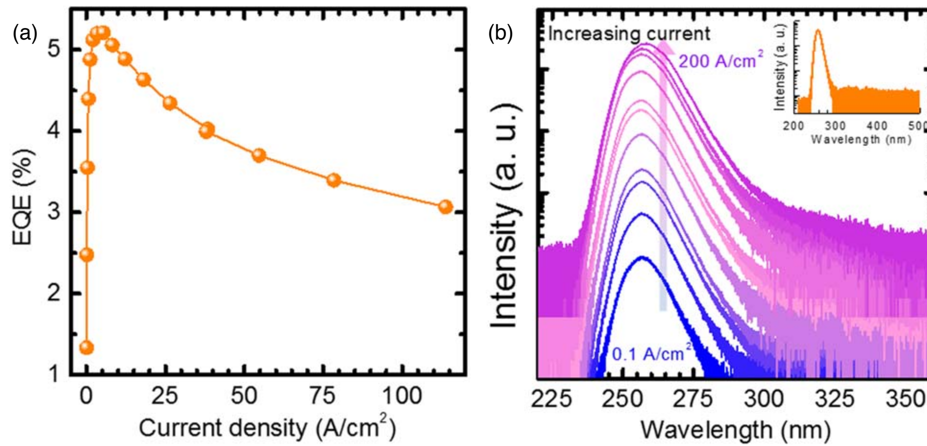

Fig. 7. (Color online) (a) Variation of EQE with current density measured under CW bias at room temperature for an AlGaN LED operating at ~255 nm. (b) EL spectra measured at different injection currents. Inset: EL spectrum at an injection current of 10 A cm^{-2} without any defect-related emission from 200 to 500 nm. (All reproduced from Ref. 41, with the permission of AIP Publishing.)

stable emission over a large range of injection currents, shown in Fig. 7(b). No defect-related emission at longer wavelengths was measured, shown in the inset of Fig. 7(b). A significant efficiency droop, however, was observed at relatively low injection currents.

TJ based UV LEDs operating at even shorter emission wavelengths (~245 nm) have also been demonstrated.[79] Device structures having different designs showed the crucial role of the electron blocking layer. Optimally designing the electron-blocking layer with the inclusion of both Mg and polarization-enhanced doping resulted in an enhancement of the EQE by over 50%, compared to a device without an electron blocking layer. These studies, together with detailed time-resolved UV optical spectroscopy, suggest that electron overflow is the primary cause of the efficiency droop of deep UV LEDs.[79]

3.1.4. Electrically pumped mid and deep UV laser diodes. To date, it has remained challenging to achieve low threshold mid and deep UV laser diodes. Moreover, there have been no demonstrations of surface emitting laser diodes in these wavelengths. In this regard, the use of dislocation-free III-nitride photonic nanocrystal arrays for realizing UV laser diodes has been studied. For example, surface emitting laser diodes can be realized by operating at the Γ point of a photonic crystal structure at which in-plane wavevector k_{xy} is nearly zero and light is largely coupled to the vertical direction.[80] Such a unique design of UV surface emitting laser does not involve the use of conventional heavily dislocated and highly resistive AlGaN-based distributed Bragg reflectors. A surface emitting green laser was recently demonstrated utilizing core-shell InGaN/GaN photonic nanocrystals, which exhibited a low threshold of ~400 A cm^{-2} at room temperature.[26] Studies further showed that III-nitride nanocrystal arrays can function as a mirrorless topological resonator,[81] which has been exploited to realize a low

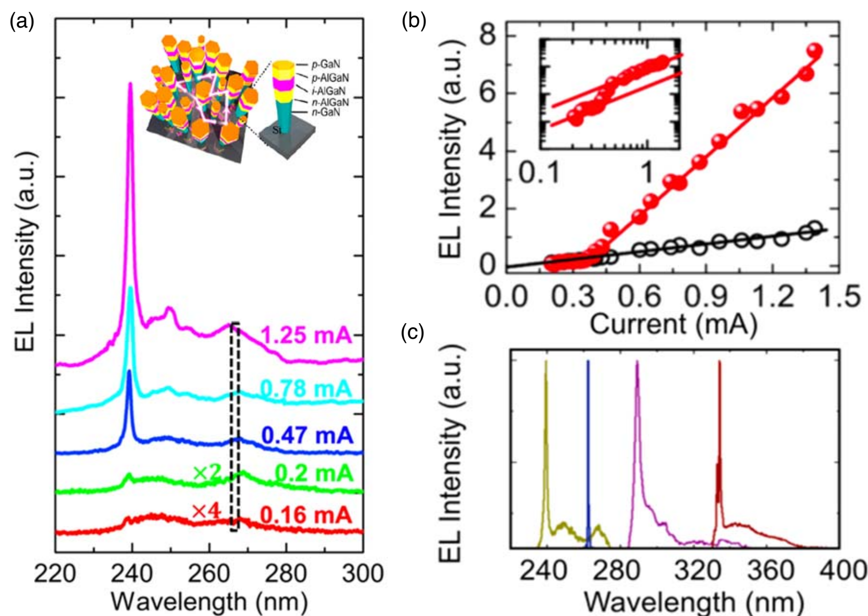

Fig. 8. (Color online) (a) Emission spectra of an AlGaN nanocrystal laser diode at 239 nm under room temperature. Schematic of the device is shown in the inset. (b) Emission intensity with current for the lasing peak (red filled circles) and a non-lasing peak (black open circles) indicated by the black dashed box in (a). (c) Emission spectra of AlGaN nanocrystal laser diodes from UV-A band to UV-C bands. (All reproduced from Ref. 51 with a Creative Commons Attribution (CC BY) license.)

 © 2021 The Japan Society of Applied Physics

threshold UV laser diode operating at 369.5 nm.[82] Owing to the dislocation-free crystalline quality, reduced surface recombination with the Al-rich shell, and topological resonance, the AlGaN photonic nanocrystal UV laser diode exhibited a threshold ~2.1 kA cm^{-2} which is significantly lower than that of previously reported GaN laser diodes in this wavelength range.[83–86] Similar effect has also been utilized to realize laser diodes operating in the UV-B and UV-C bands.[20,21,87,88] An AlGaN nanocrystal laser diode operating at 239 nm was demonstrated at room temperature.[21] Schematic of the device is illustrated in the inset of Fig. 8(a). The emission spectra under various injection currents are shown in Fig. 8(a). A broad spontaneous emission was measured under a low injection current while a narrow and pronounced peak emerged at 239 nm as the current increased. The variation of the output power with current is shown in Fig. 8(b), demonstrating a clear threshold ~0.35 mA. An S-shape curve, shown in the log-scale plot in the inset, was clearly measured. Detailed measurements confirmed that the intensity of the background emission (black circles) showed negligible increase with injection current, which further supports the achievement of lasing. The lasing spectra of some recently reported AlGaN photonic nanocrystal laser diodes operating from UV-A to UV-C are shown in Fig. 8(c).[51]

3.2. Discussion

Nanoscale and quantum engineering provides new opportunities to break the efficiency bottleneck of UV-C and far UV-C optoelectronics. Several critical challenges, however, need to be further addressed for their practical application. Currently reported high efficiency UV-C LEDs generally exhibit severe efficiency droop at relatively low current densities. Detailed electrical and optical measurements suggested that the efficiency droop was largely due to electron overflow, instead of Auger recombination.[41,79] Such a critical issue can be potentially addressed by optimizing the electron blocking layer and by improving p-type conductivity. Techniques such as metal–semiconductor junction-assisted epitaxy and TJ structures have been actively pursued. Utilizing a combination of these methods along with techniques such as polarization doping has been shown to significantly improve the performance of deep UV LEDs.[79] In addition, co-doping of III-nitrides with Mg, O, In and Be has been shown to improve the hole concentration.[89–91] These efforts can be revisited for Al-rich AlGaN, especially considering the fact that Be has been theorized to be a better acceptor dopant as compared to Mg for AlN.[92–94] It should also be noted that most of the work on AlGaN UV LEDs is based on materials grown in the metal-polar orientation. N-polar structures, however, may offer some unique advantages, including enhanced carrier transport and suppressed electron overflow.[95–97]

The light extraction efficiency (LEE), especially in the deep UV spectrum where transverse magnetic polarized emission in the horizontal directions dominates, can also be improved by incorporating photonic crystal to couple emitted light to the vertical direction.[98] The diameter and spacing of nanocrystal can be designed to form a photonic crystal with the Γ point matching the emission peak wavelength. Compared to a low LEE of less than 10% around 240 nm for conventional planar LED structures, the LEE can be improved to above 80%, which is also highly robust with variations of the design parameters.

Critical to the progress of UV-C and far UV-C laser diodes is the significant reduction of lasing threshold and improvement of output power under continuous wave operation. In this regard, it is essential to achieve efficient hole injection and transport in the device active region. Moreover, the threshold current of AlGaN-based UV laser diodes is ultimately limited by the large density of states and large carrier density required for population inversion in conventional AlGaN quantum wells. The realization of three-dimensional quantum confinement of charge carriers in Al-rich AlGaN offers unique opportunities to significantly increase the differential gain of UV laser diodes, thereby drastically reducing the lasing threshold. In this regard, promising progress in UV laser diodes has been made by exploiting such nanostructures.[20,21,87,88] Future studies include the design and development of both edge- and surface-emitting laser diodes with the use of TJ, improved p-type conduction, and photonic bandgap engineering to realize both low threshold and high power operation over a broad range of UV spectrum.

4. Conclusions

Developing high efficiency all-solid-state UV-C and far UV-C light sources is a critical and urgent need to combat the ongoing pandemic and to deal with similar situations in the future. To date, however, it has remained a daunting challenge. Recent advances of nanoscale and quantum engineering of AlGaN semiconductors have offered new opportunities and perspectives to address some of the most critical challenges at the materials, physics, and device engineering levels. Significant advantages offered by AlGaN nanostructures include relatively efficient p-type conduction, three-dimensional quantum confinement of charge carriers, and photonic bandgap engineering. It is expected that further understanding of the physics, epitaxy, and characteristics of III-nitride nanostructures and improvement and optimization of the device design, engineering, and integration will provide a path for the realization of high efficiency all-solid-state UVC light sources.

Acknowledgments

This work was supported by Natural Sciences and Engineering Research Council of Canada (NSERC), U.S. Army Research Office, National Science Foundation, and College of Engineering, University of Michigan.

Conflict of interest

Some IP related to this work was licensed to NS Nanotech, which was co-founded by Z. Mi. The University of Michigan has a financial interest in NS Nanotech, Inc.

1) S. E. Beck, H. Ryu, L. A. Boczek, J. L. Cashdollar, K. M. Jeanis, J. S. Rosenblum, O. R. Lawal, and K. G. Linden, Water Res. **109**, 207 (2017).

2) A. M. Zyara, H. Heinonen-Tanski, A.-M. Veijalainen, and E. Torvinen, Water. **9**, 46 (2017).

3) M. A. Khan, R. Takeda, Y. Yamada, N. Maeda, M. Jo, and H. Hirayama, Opt. Lett. **45**, 495 (2020).

 © 2021 The Japan Society of Applied Physics

4) M. A. Khan, E. Matsuura, Y. Kashima, and H. Hirayama, Jpn. J. Appl. Phys. **59**, SAAD01 (2019).
5) H. Hirayama, Y. Tsukada, T. Maeda, and N. Kamata, Appl. Phys. Express **3**, 031002 (2010).
6) M. A. Khan, N. Maeda, M. Jo, Y. Akamatsu, R. Tanabe, Y. Yamada, and H. Hirayama, J. Mater. Chem. C **7**, 143 (2019).
7) T. H. Lee, T. H. Park, H. W. Shin, N. Maeda, M. Jo, H. Hirayama, B.-H. Kim, and T. G. Kim, Adv. Opt. Mater. **8**, 1901430 (2020).
8) J. Yun, Y. Kashima, and H. Hirayama, AIP Adv. **8**, 125126 (2018).
9) H. Hideki, M. Noritoshi, F. Sachie, T. Shiro, and K. Norihiko, Jpn. J. Appl. Phys. **53**, 100209 (2014).
10) H. Hirayama, S. Fujikawa, N. Noguchi, J. Norimatsu, T. Takano, K. Tsubaki, and N. Kamata, Phys. Status Solidi A **206**, 1176 (2009).
11) H. Hirayama, T. Yatabe, N. Noguchi, T. Ohashi, and N. Kamata, Phys. Status Solidi C **5**, 2969 (2008).
12) S. Tanaka et al., Appl. Phys. Express **13**, 045504 (2020).
13) K. Sato et al., Appl. Phys. Express **13**, 031004 (2020).
14) Z. Zhang, M. Kushimoto, T. Sakai, N. Sugiyama, L. J. Schowalter, C. Sasaoka, and H. Amano, Appl. Phys. Express **12**, 124003 (2019).
15) S. Zhao, S. Y. Woo, M. Bugnet, X. Liu, J. Kang, G. A. Botton, and Z. Mi, Nano Lett. **15**, 7801 (2015).
16) A. T. Connie, S. Zhao, S. M. Sadaf, I. Shih, Z. Mi, X. Du, J. Lin, and H. Jiang, Appl. Phys. Lett. **106**, 213105 (2015).
17) D. A. Laleyan, S. Zhao, S. Y. Woo, H. N. Tran, H. B. Le, T. Szkopek, H. Guo, G. A. Botton, and Z. Mi, Nano Lett. **17**, 3738 (2017).
18) A. Pandey, X. Liu, Z. Deng, W. Shin, D. Laleyan, K. Mashooq, E. Reid, E. Kioupakis, P. Bhattacharya, and Z. Mi, Phys. Rev. Mater. **3**, 053401 (2019).
19) A. Pandey, W. J. Shin, J. Gim, R. Hovden, and Z. Mi, Photon. Res. **8**, 331 (2020).
20) S. Zhao et al., Sci. Rep. **5**, 8332 (2015).
21) S. Zhao, X. Liu, Y. Wu, and Z. Mi, Appl. Phys. Lett. **109**, 191106 (2016).
22) V. Consonni, M. Hanke, M. Knelangen, L. Geelhaar, A. Trampert, and H. Riechert, Phys. Rev. B **83**, 035310 (2011).
23) V. Consonni, M. Knelangen, L. Geelhaar, A. Trampert, and H. Riechert, Phys. Rev. B **81**, 085310 (2010).
24) X. Liu, B. H. Le, S. Y. Woo, S. Zhao, A. Pofelski, G. A. Botton, and Z. Mi, Opt. Express **25**, 30494 (2017).
25) H. Sekiguchi, K. Kishino, and A. Kikuchi, Appl. Phys. Express **1**, 124002 (2008).
26) Y.-H. Ra, R. T. Rashid, X. Liu, S. M. Sadaf, K. Mashooq, and Z. Mi, Sci. Adv. **6**, eaav7523 (2020).
27) N. H. Tran, B. H. Le, S. Zhao, and Z. Mi, Appl. Phys. Lett. **110**, 032102 (2017).
28) Y. Wu, X. Liu, P. Wang, D. A. Laleyan, K. Sun, Y. Sun, C. Ahn, M. Kira, E. Kioupakis, and Z. Mi, Appl. Phys. Lett. **116**, 013101 (2020).
29) A. Aiello et al., Nano Lett. **19**, 7852 (2019).
30) E. Francesco Pecora, W. Zhang, A. Yu. Nikiforov, L. Zhou, D. J. Smith, J. Yin, R. Paiella, L. Dal Negro, and T. Moustakas, Appl. Phys. Lett. **100**, 061111 (2012).
31) E. Francesco Pecora, W. Zhang, A. Y. Nikiforov, J. Yin, R. Paiella, L. Dal Negro, and T. D. Moustakas, J. Appl. Phys. **113**, 013106 (2013).
32) J. Ristić, E. Calleja, S. Fernández-Garrido, L. Cerutti, A. Trampert, U. Jahn, and K. H. Ploog, J. Cryst. Growth **310**, 4035 (2008).
33) V. Consonni, A. Trampert, L. Geelhaar, and H. Riechert, Appl. Phys. Lett. **99**, 033102 (2011).
34) K. Hestroffer, C. Leclere, C. Bougerol, H. Renevier, and B. Daudin, Phys. Rev. B **84**, 245302 (2011).
35) K. A. Bertness, A. W. Sanders, D. M. Rourke, T. E. Harvey, A. Roshko, J. B. Schlager, and N. A. Sanford, Adv. Funct. Mater. **20**, 2911 (2010).
36) M. D. Brubaker, S. M. Duff, T. E. Harvey, P. T. Blanchard, A. Roshko, A. W. Sanders, N. A. Sanford, and K. A. Bertness, Cryst. Growth Des. **16**, 596 (2016).
37) M. D. Brubaker, K. L. Genter, A. Roshko, P. T. Blanchard, B. T. Spann, T. E. Harvey, and K. A. Bertness, Nanotechnology **30**, 234001 (2019).
38) A. Bengoechea-Encabo, F. Barbagini, S. Fernandez-Garrido, J. Grandal, J. Ristic, M. A. Sanchez-Garcia, E. Calleja, U. Jahn, E. Luna, and A. Trampert, J. Cryst. Growth **325**, 89 (2011).
39) Ž. Gačević, D. Gómez Sánchez, and E. Calleja, Nano Lett. **15**, 1117 (2015).
40) K. Kishino, H. Sekiguchi, and A. Kikuchi, J. Cryst. Growth **311**, 2063 (2009).
41) A. Pandey, J. Gim, R. Hovden, and Z. Mi, Appl. Phys. Lett. **117**, 241101 (2020).
42) E. Iliopoulos and T. Moustakas, Appl. Phys. Lett. **81**, 295 (2002).
43) T. D. Moustakas and A. Bhattacharyya, Phys. Status Solidi C **9**, 580 (2012).
44) C. G. Van de Walle and J. Neugebauer, J. Appl. Phys. **95**, 3851 (2004).
45) C. G. Van de Walle, C. Stampfl, and J. Neugebauer, J. Cryst. Growth **189**, 505 (1998).
46) C. G. Van de Walle, C. Stampfl, J. Neugebauer, M. McCluskey, and N. Johnson, MRS Internet J. Nitride Semicond. Res. **4**, 890 (1999).
47) Y. Liang and E. Towe, J. Appl. Phys. **123**, 095303 (2018).
48) Y.-H. Liang and E. Towe, Appl. Phys. Rev. **5**, 011107 (2018).
49) X. Liu, F. A. Chowdhury, S. Vanka, S. Chu, and Z. Mi, Phys. Status Solidi A **217**, 1900885 (2020).
50) K. B. Nam, M. L. Nakarmi, J. Li, J. Y. Lin, and H. X. Jiang, Appl. Phys. Lett. **83**, 878 (2003).
51) S. Zhao and Z. Mi, Crystals **7**, 268 (2017).
52) M. L. Nakarmi, N. Nepal, C. Ugolini, T. M. Altahtamouni, J. Y. Lin, and H. X. Jiang, Appl. Phys. Lett. **89**, 152120 (2006).
53) Z. Bryan, I. Bryan, B. E. Gaddy, P. Reddy, L. Hussey, M. Bobea, W. Guo, M. Hoffmann, R. Kirste, and J. Tweedie, Appl. Phys. Lett. **105**, 222101 (2014).
54) P. Reddy, M. Hoffmann, F. Kaess, Z. Bryan, I. Bryan, M. Bobea, A. Klump, J. Tweedie, R. Kirste, and S. Mita, J. Appl. Phys. **120**, 185704 (2016).
55) K. Alberi and M. A. Scarpulla, Sci. Rep. **6**, 27954 (2016).
56) C. Stampfl and C. Van de Walle, Phys. Rev. B **65**, 155212 (2002).
57) C. Stampfl and C. G. Van de Walle, Appl. Phys. Lett. **72**, 459 (1998).
58) S. Nakamura, Science **281**, 956 (1998).
59) Y. Xing, D. Zhao, D. Jiang, Z. Liu, J. Zhu, P. Chen, J. Yang, F. Liang, S. Liu, and L. Zhang, Nanoscale Res. Lett. **14**, 88 (2019).
60) D. Bayerl, S. M. Islam, C. M. Jones, V. Protasenko, D. Jena, and E. Kioupakis, Appl. Phys. Lett. **109**, 241102 (2016).
61) D. Ma et al., Sci. Rep. **7**, 5843 (2017).
62) C. He, Z. Qin, F. Xu, M. Hou, S. Zhang, L. Zhang, X. Wang, W. Ge, and B. Shen, Sci. Rep. **5**, 13046 (2015).
63) J. E. Fouquet and A. E. Siegman, Appl. Phys. Lett. **46**, 280 (1985).
64) Y. Taniyasu, M. Kasu, and T. Makimoto, Nature **441**, 325 (2006).
65) S. Zhao, M. Djavid, and Z. Mi, Nano Lett. **15**, 7006 (2015).
66) R. Dahal, J. Li, S. Majety, B. N. Pantha, X. K. Cao, J. Y. Lin, and H. X. Jiang, Appl. Phys. Lett. **98**, 211110 (2011).
67) C. Attaccalite, M. Bockstedte, A. Marini, A. Rubio, and L. Wirtz, Phys. Rev. B **83**, 144115 (2011).
68) W. Orellana and H. Chacham, Phys. Rev. B **63**, 125205 (2001).
69) V. Wang, R. J. Liu, H. P. He, C. M. Yang, and L. Ma, Solid State Commun. **177**, 74 (2014).
70) Y. Taniyasu and M. Kasu, Appl. Phys. Lett. **98**, 131910 (2011).
71) S. Zhao, S. Y. Woo, S. M. Sadaf, Y. Wu, A. Pofelski, D. A. Laleyan, R. T. Rashid, Y. Wang, G. A. Botton, and Z. Mi, APL Mater. **4**, 086115 (2016).
72) Y. Zhang, S. Krishnamoorthy, F. Akyol, A. A. Allerman, M. W. Moseley, A. M. Armstrong, and S. Rajan, Appl. Phys. Lett. **109**, 121102 (2016).
73) Y. Zhang, S. Krishnamoorthy, J. M. Johnson, F. Akyol, A. Allerman, M. W. Moseley, A. Armstrong, J. Hwang, and S. Rajan, Appl. Phys. Lett. **106**, 141103 (2015).
74) S. M. Sadaf, Y. H. Ra, H. P. T. Nguyen, M. Djavid, and Z. Mi, Nano Lett. **15**, 6696 (2015).
75) A. T. M. G. Sarwar, B. J. May, J. I. Deitz, T. J. Grassman, D. W. McComb, and R. C. Myers, Appl. Phys. Lett. **107**, 101103 (2015).
76) S. M. Sadaf, Y. H. Ra, T. Szkopek, and Z. Mi, Nano Lett. **16**, 1076 (2016).
77) S. M. Sadaf, S. Zhao, Y. Wu, Y. H. Ra, X. Liu, S. Vanka, and Z. Mi, Nano Lett. **17**, 1212 (2017).
78) S. Zhao, S. M. Sadaf, S. Vanka, Y. Wang, R. Rashid, and Z. Mi, Appl. Phys. Lett. **109**, 201106 (2016).
79) A. Pandey, J. Gim, R. Hovden, and Z. Mi, Appl. Phys. Lett. **118**, 241109 (2021).
80) M. Imada, A. Chutinan, S. Noda, and M. Mochizuki, Phys. Rev. B **65**, 195306 (2002).
81) R. Merlin and S. M. Young, Opt. Express **22**, 18579 (2014).
82) B. H. Le, X. Liu, N. H. Tran, S. Zhao, and Z. Mi, Opt. Express **27**, 5843 (2019).
83) H. Matsubara, S. Yoshimoto, H. Saito, Y. Jianglin, Y. Tanaka, and S. Noda, Science **319**, 445 (2008).
84) Y. Aoki, M. Kuwabara, Y. Yamashita, Y. Takagi, A. Sugiyama, and H. Yoshida, Appl. Phys. Lett. **107**, 151103 (2015).
85) H. Yoshida, M. Kuwabara, Y. Yamashita, Y. Takagi, K. Uchiyama, and H. Kan, New J. Phys. **11**, 125013 (2009).
86) H. Yoshida, M. Kuwabara, Y. Yamashita, K. Uchiyama, and H. Kan, Phys. Status Solidi A **208**, 1586 (2011).
87) K. H. Li, X. Liu, Q. Wang, S. Zhao, and Z. Mi, Nat. Nanotechnol. **10**, 140 (2015).
88) S. Zhao, X. Liu, S. Y. Woo, J. Kang, G. A. Botton, and Z. Mi, Appl. Phys. Lett. **107**, 043101 (2015).

© 2021 The Japan Society of Applied Physics

89) A.-M. Siladie, G. Jacopin, A. Cros, N. Garro, E. Robin, D. Caliste, P. Pochet, F. Donatini, J. Pernot, and B. Daudin, Nano Lett. **19**, 8357 (2019).
90) F. Naranjo, M. Sánchez-García, J. Pau, A. Jimenez, E. Calleja, E. Munoz, J. Oila, K. Saarinen, and P. Hautojarvi, Phys. Status Solidi A **180**, 97 (2000).
91) G. Kipshidze, V. Kuryatkov, B. Borisov, Y. Kudryavtsev, R. Asomoza, S. Nikishin, and H. Temkin, Appl. Phys. Lett. **80**, 2910 (2002).
92) A. Sedhain, T. Al Tahtamouni, J. Li, J. Lin, and H. Jiang, Appl. Phys. Lett. **93**, 141104 (2008).
93) R. Wu, L. Shen, M. Yang, Z.-D. Sha, Y. Cai, Y. P. Feng, Z. Huang, and Q. Y. Wu, Appl. Phys. Lett. **91**, 152110 (2007).
94) F. Mireles and S. E. Ulloa, Phys. Rev. B **58**, 3879 (1998).
95) Z. Zhuang, D. Iida, and K. Ohkawa, Opt. Express **28**, 30423 (2020).
96) H. Tao, S. Xu, J. Zhang, P. Li, Z. Lin, and Y. Hao, IEEE Trans. Electron Devices **66**, 478 (2018).
97) J. Verma, J. Simon, V. Protasenko, T. Kosel, H. Grace Xing, and D. Jena, Appl. Phys. Lett. **99**, 171104 (2011).
98) X. Liu, K. Mashooq, T. Szkopek, and Z. Mi, IEEE Photonics J. **10**, 4501211 (2018).

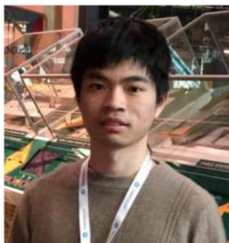

Dr. Xianhe Liu received his Bachelor's degree from Huaqiao University, China in 2012 and his Ph.D. degree from McGill University, Canada in 2019. Then he started working as a postdoctoral researcher in Prof. Zetian Mi's lab in the University of Michigan, Ann Arbor. He is currently a professor at Xidian University. His research interests include the molecular beam epitaxial growth of III-nitride nanostructures, nanofabrication and simulation design of optoelectronic devices.

Dr. Ayush Pandey graduated from the Electrical Engineering program at the Indian Institute of Technology, Kanpur, India in 2015, and he received his doctoral degree in Electrical and Computer Engineering from the University of Michigan, Ann Arbor in 2021. He is currently working on the epitaxy, characterization and fabrication of III-nitride devices.

Dr. Zetian Mi is a Professor in the Department of Electrical Engineering and Computer Science at the University of Michigan, Ann Arbor. He received a Ph.D. degree in Applied Physics at the University of Michigan in 2006. His teaching and research interests are in the areas of III-nitride semiconductors, LEDs, lasers, quantum photonics, solar fuels, and artificial photosynthesis. He was a faculty member at McGill University from 2007 to 2016, where he received several awards, including the Hydro-Québec Nano-Engineering Scholar Award in 2009, the William Dawson Scholar Award in 2011, the Christophe Pierre Award for Research Excellence in 2012, and the Engineering Innovation Award in 2015. Prof. Mi has received the Science and Engineering Award from W. M. Keck Foundation in 2020 and the David E. Liddle Research Excellence Award in 2021. Prof. Mi has also received the Young Investigator Award from the 27th North American molecular beam epitaxy (MBE) Conference in 2010, the Young Scientist Award from the International Symposium on Compound Semiconductors in 2015, and the IEEE Photonics Society Distinguished Lecturer Award in 2020. Prof. Mi currently serves as the Editor of *Progress in Quantum Electronics*. Prof. Mi is a fellow of SPIE and OSA. Prof. Mi is a co-founder and member of the Board of Directors of NS Nanotech, Inc.

© 2021 The Japan Society of Applied Physics